BIOCHEMISTRY
including biophysical chemistry & molecular biology

Article

pubs.acs.org/biochemistry

Reversible Phenol Oxidation and Reduction in the Structurally Well-Defined 2-Mercaptophenol-α_3C Protein

Cecilia Tommos,* Kathleen G. Valentine, Melissa C. Martínez-Rivera, Li Liang, and Veronica R. Moorman

Graduate Group in Biochemistry and Molecular Biophysics and Department of Biochemistry and Biophysics, University of Pennsylvania, Philadelphia, Pennsylvania 19104-6059, United States

Supporting Information

ABSTRACT: 2-Mercaptophenol-α_3C serves as a biomimetic model for enzymes that use tyrosine residues in redox catalysis and multistep electron transfer. This model protein was tailored for electrochemical studies of phenol oxidation and reduction with specific emphasis on the redox-driven protonic reactions occurring at the phenol oxygen. This protein contains a covalently modified 2-mercaptophenol-cysteine residue. The radical site and the phenol compound were specifically chosen to bury the phenol OH group inside the protein. A solution nuclear magnetic resonance structural analysis (i) demonstrates that the synthetic 2-mercaptophenol-α_3C model protein behaves structurally as a natural protein, (ii) confirms the design of the radical site, (iii) reveals that the ligated phenol forms an interhelical hydrogen bond to glutamate 13 (phenol oxygen−carboxyl oxygen distance of 3.2 ± 0.5 Å), and (iv) suggests a proton-transfer pathway from the buried phenol OH (average solvent accessible surface area of 3 ± 5%) via glutamate 13 (average solvent accessible surface area of the carboxyl oxygens of 37 ± 18%) to the bulk solvent. A square-wave voltammetry analysis of 2-mercaptophenol-α_3C further demonstrates that (v) the phenol oxidation−reduction cycle is reversible, (vi) formal phenol reduction potentials can be obtained, and (vii) the phenol-O$^\bullet$ state is long-lived with an estimated lifetime of ≥180 millisecond. These properties make 2-mercaptophenol-α_3C a unique system for characterizing phenol-based proton-coupled electron transfer in a low-dielectric and structured protein environment.

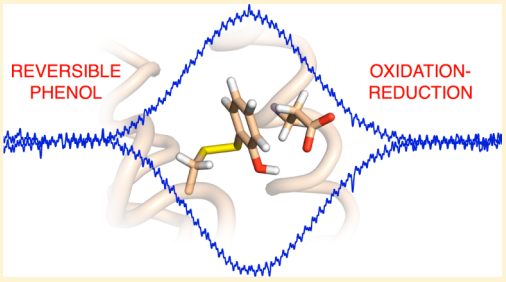

Tyrosine serves as a one-electron redox cofactor in proteins and may form three redox pairs: Y-OH$^{\bullet+}$/Y-OH, Y-O$^\bullet$/Y-OH, and Y-O$^\bullet$/Y-O$^-$.[1−5] The pK_a values of aqueous tyrosine in its oxidized and reduced state are −2 and 10, respectively. This predicts that Y-O$^\bullet$/Y-OH is the dominating redox couple in a protein environment.[1] Thus, oxidation and reduction of protein tyrosine residues is coupled to de- and reprotonation at the phenol oxygen. Mechanistically, these electron and proton transfers may occur along concerted or stepwise pathways, and significant efforts are being made to experimentally characterize these types of proton-coupled electron-transfer (PCET) reactions and form a theoretical framework for PCET processes in proteins.[4−10]

The model approach to studying tyrosine-based PCET ranges from free phenol in neat water to engineering of natural proteins (e.g., refs 11−25). The de novo α_3X radical proteins were developed as part of this effort.[3,26,27] Scheme 1 shows the amino acid sequence of the three-helix bundle that forms the structural platform for the α_3X system.

GSR(1)·**V**K**A**L**E**E**K**·**V**K**A**L**E**E**K**·**V**K-*A**L**GGGG*-R·**I**E**E**L**

K**K**K·**X**(**32**)E**E**L**K**K**K**·**I**E**E**-*L**GGGGE* -·**V**K**K**V**E**E**E**·**V**K**K**L**

E**E**E·**I**K**K***L*(65) (1)

The sequence is based on the classic heptad-repeat design of α-helical coiled coils and bundles.[28] The seven-residue heptads, with internal positions labeled *a*−*g*, are marked by dots. The N-terminal GS residues (italic) form part of a thrombin cleavage site and are labeled as −2 and −1 to keep the amino acid numbering consistent between the chemically synthesized (65 residues[26]) and recombinantly expressed (66 or 67 residues[29,30]) α_3X proteins. The radical site (position 32, bold) is located in the middle of the central helix and occupied by a tyrosine (to form the α_3Y protein), a cysteine (α_3C), or a tryptophan (α_3W).

α_3Y is an electrochemically reversible system with a long-lived tyrosine radical.[31] The radical site in α_3Y was designed to completely shield Y32 from the bulk solvent.[26,32] Here we describe an α_3X variant with a more detailed design of the radical site. Our goal was to develop a system in which the degree of solvent interactions at the phenol OH can be manipulated experimentally. To facilitate subsequent electrochemical analyses of the radical system, it is important to make well-defined structural changes as recently discussed and demonstrated for α_3Y.[31,32] The key challenge is thus to

Received: December 1, 2012
Revised: January 27, 2013
Published: February 1, 2013

dx.doi.org/10.1021/bi301613p | *Biochemistry* 2013, 52, 1409−1418

construct a system in which the solvent exposure of the phenol OH is modulated *specifically* while changes in other structural interactions, both global to the protein scaffold and local to the radical site, are *kept to a minimum*. Moving the single tyrosine between different sites in α_3Y is expected to change the solvent exposure of the phenol OH but would most likely also result in significant changes in other interactions, e.g., electrostatic forces, experienced by the phenol ring. For this reason, position 32 was made into a phenol-binding site with the purpose of making the location of the phenol OH group flexible while the location of the aromatic ring itself remains relatively fixed. Panels A and B of Figure 1 provide a cartoon description of the

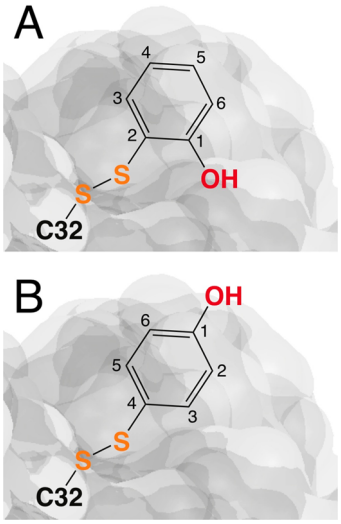

Figure 1. Cartoon description of the (A) 2-mercaptophenol-α_3C (2MP-α_3C) and (B) 4-mercaptophenol-α_3C (4MP-α_3C) protein design.[30] The main purpose when constructing these proteins was to make significant changes in the solvent exposure of the phenol OH group while keeping other structural changes, both in the overall protein scaffold and at the radical site, to a minimum.

design behind the mercaptophenol-α_3C (MP-α_3C) proteins.[30] It is based on the balance of two predictions: (i) that the hydrophobic packing pattern of the three-helix bundle is maintained[29] and, consequently, that C32 resides inside the folded protein and (ii) that the OH of the ligated phenol is oriented toward the protein surface to minimize the energetic cost of solvating the polar group inside the low-dielectric protein medium. If these predictions hold, the short distance between the OH and the protein-ligating sulfur atom in 2MP will ensure a buried position of the OH (Figure 1A). In contrast, the longer distance between the OH and SH in 4MP may result in a system where C32 is buried while the phenol OH resides close to or at the protein surface (Figure 1B). In an earlier report, we described a protocol for generating 2-, 3-, and 4MP-α_3C and provided a preliminary structural and electrochemical characterization of these three proteins.[30] Here we present the solution nuclear magnetic resonance (NMR) structure of 2MP-α_3C and confirm the design of the radical site. The structural analysis further suggests a proton-transfer pathway from the buried phenol OH via a hydrogen-bonded glutamate to the bulk solvent. We show that 2MP-α_3C can be reversibly oxidized and reduced and that the phenol has a radical lifetime ($t_{1/2}$) on the millisecond time scale. We conclude that the 2MP-α_3C system is uniquely suited for the electrochemical characterization of PCET reactions associated with phenol oxidation and reduction in a well-defined protein environment.

MATERIALS AND METHODS

Expression and Purification of α_3C. α_3C was expressed as a thioredoxin fusion using a modified pET15 vector (Novagen) transformed into BL21-CodonPlus(DE3)-RIL (Stratagene). Cells were induced with 1 mM IPTG for 3 h at 37 °C in LB medium or for 24 h at 30 °C in minimal medium containing $^{15}NH_4Cl$ and uniformly labeled [^{13}C]glucose (Cambridge Isotope Laboratories). Minimal medium containing $^{15}NH_4Cl$, 10% ^{13}C-labeled glucose, and 90% unlabeled glucose provided the samples used for prochiral methyl assignments.[33] Harvested cells were resuspended in 20 mM Tris-HCl, 500 mM NaCl, and 5 mM imidazole (pH 7.9), treated with lysozyme for 30 min, and lysed by sonication. The lysate was clarified by centrifugation and passed over a nickel column (His·bind resin, EMD Millipore), and the thioredoxin-α_3C fusion protein was eluted via a 0 to 400 mM imidazole gradient. Thrombin (T6634, Sigma-Aldrich) was added to the fusion protein fraction and the resulting mixture dialyzed against 50 mM Tris-HCl, 500 mM NaCl, and 2.5 mM $CaCl_2$ (pH 8.0) at room temperature overnight. The digestion mixture was passed over a second nickel column to remove the His-tagged thioredoxin and any remaining undigested fusion protein. α_3C was isolated by reverse-phase high-performance liquid chromatography (HPLC) (TP2181010 column, Grace/Vydac) using an acetonitrile/water gradient containing 0.1% (w/v) trifluoroacetic acid and stored as lyophilized powder.

Preparation of 2-Mercaptophenol-α_3C. Lyophilized α_3C was dissolved in 50 mM potassium phosphate and 3.0 M guanidinium hydrochloride (pH 8.0). Dithiothreitol was added at an estimated 5−10-fold excess and the mixture incubated for 15 min at room temperature. The buffer was exchanged using PD-10 columns (GE Healthcare) equilibrated in 50 mM potassium phosphate (pH 8.0) and the protein concentration determined immediately by an Ellman's assay [5,5′-dithiobis(2-nitrobenzoic acid), Sigma-Aldrich][34] under denaturing conditions using an ε_{412} of 37000 M^{-1} cm^{-1}. The binding reaction mixture was prepared as follows: 1 part α_3C dissolved in 50 mM potassium phosphate, 10 parts 2-mercaptophenol (Sigma-Aldrich), and 3 M guanidinium hydrochloride. The pH was adjusted to 8.0 and the sample placed on a rotisserie at 4 °C overnight. The binding mixture was dialyzed against 50 mM acetate and 30 mM KCl (pH 6.0) at 4 °C for 24 h and purified by reverse-phase HPLC, and the 2MP-α_3C protein was stored as lyophilized powder. The concentration of 2MP-α_3C was determined using an ε_{290} of 3700 M^{-1} cm^{-1}.[30]

NMR Spectroscopy. NMR spectra were collected at 25 °C on a 500 MHz Bruker Advance III spectrometer (pulsed field gradient diffusion experiments) and 30 °C on a 750 MHz Varian Inova spectrometer (all other experiments). Both spectrometers were equipped with cold probes. Sample conditions were as follows: (i) pulsed field gradient diffusion experiments, 440 μM 2MP-α_3C in 20 mM deuterated sodium acetate, 20 mM potassium phosphate, 20 mM sodium borate, 80 mM KCl, and 5% D_2O (pH* 6.6) (glass electrode pH reading uncorrected for deuterium isotope effects); (ii) two-dimensional (2D) ^{1}H−^{1}H NOESY, 800 μM 2MP-α_3C in 30 mM deuterated sodium acetate, 30 mM KCl, 250 μM 4,4-dimethyl-4-silapentane-1-sulfonic acid (DSS), and 99.99% D_2O (pH* 5.5); (iii) prochiral methyl assignments, 800 μM 10% ^{13}C-labeled 2MP-α_3C in 30 mM deuterated sodium acetate, 30

mM KCl, 250 μM DSS, and 99.99% D_2O (pH* 5.5); (iv) all other experiments, 800 μM ^{13}C- and ^{15}N-labeled 2MP-α_3C dissolved in 30 mM deuterated sodium acetate, 30 mM KCl, and 250 μM DSS buffer (pH* 5.5) containing either 10 or 99.99% D_2O. Pulsed field gradient diffusion experiments for measuring the diffusion coefficient of 2MP-α_3C were conducted as described in ref 35. Backbone N, H, C, and CA and side chain CB resonance assignments were derived from analyses of triple-resonance three-dimensional (3D) HNCO, HNCACB, and CBCA(CO)NH experiments.[36] Side chain resonance assignments were obtained from 3D CC(CO)NH-TOCSY, H(CC)(CO)NH-TOCSY, and HCCH-TOCSY data.[36] The completeness of the backbone (99%) and side chain (96%) resonance assignments was evaluated using the Assignment Validation Suite (AVS) webserver.[37] Prochiral methyl assignments (100% completeness) were performed using the trace glucose labeling strategy.[33] Backbone ϕ and ψ torsion angle restraints were obtained from backbone N, C, CA, and HA and side chain CB chemical shifts using TALOS.[38] The predicted ϕ angles were confirmed by a 3D HNHA experiment.[39] NOE distance restraints were derived from 3D NOESY-$^{15}N-^{1}H$ HSQC (collected in H_2O) and four-dimensional $^{13}C-^{1}H$ HMQC-NOESY-$^{13}C-^{1}H$ HMQC (collected in D_2O) spectra.[36,40] NOEs between protons associated with the 2-mercaptophenol ring and aliphatic protons were obtained from 2D $^{1}H-^{1}H$ NOESY and 3D NOESY-$^{13}C-^{1}H$ HSQC data (collected in D_2O).[36] The mixing time was 140 ms for all NOESY experiments. Proton chemical shifts were referenced to DSS directly and ^{13}C and ^{15}N chemical shifts indirectly. NMR data were processed using Felix95 (Accelrys Inc., San Diego, CA) and analyzed with SPARKY.[41]

Structure Calculations. Structures were generated from experimental NMR restraints by simulated annealing molecular dynamics using the Crystallography & NMR System (CNS).[42] NOE-derived proton−proton distance restraints were grouped in distance ranges of 1.7−3.0, 1.7−4.0, and 1.7−5.0 Å corresponding to strong, medium, and weak NOE cross-peak intensities, respectively. When one or two methyl groups were involved, the upper boundary was increased by 0.5 or 1.0 Å, respectively. Backbone torsion angle and H-bond restraints were derived from the secondary structure predictions made by the TALOS/HNHA analysis. One thousand trial structures were generated and further evaluated using the CNS accept.inp script to obtain a collection of 141 refined structures. The 32 lowest-energy structures from this collection form the deposited structural ensemble. Solvent accessible surface area (SASA) analyses were performed using MOLMOL,[43] and a Random Coil Index analysis was performed using the RCI webserver.[44] Structural depictions were generated using PyMOL (Schrödinger, LLC).

Data Deposition. NMR chemical shifts have been deposited in the Biological Magnetic Resonance data bank (BMRB, http://www.bmrb.wisc.edu) as entry 18703. Coordinates of the 32 lowest-energy structures have been deposited in the Protein Data Bank (PDB, http://www.rcsb.org) as entry 2LXY. In the BMRB and PDB, the covalently attached 2-mercaptophenol is treated as a ligand named HTS with a residue sequence number of 101. Table S1 of the Supporting Information correlates the residue and atom designations used in the BMRB and RCSB with the nomenclature used here and in our earlier study of 2MP-α_3C.[30]

Electrochemistry. Differential pulse voltammetry (DPV)[45,46] and square-wave voltammetry (SWV)[46−48] were performed using an Autolab PGSTAT12 potentiostat equipped with a temperature-controlled, Faraday-cage protected three-electrode microcell (Princeton Applied Research). The Ag/AgCl reference electrode and the platinum wire counter electrode (Advanced Measurements Inc.) were stored dry and prepared by filling the former with a 3 M KCl/saturated AgCl solution and the latter with sample buffer. All measurements were taken using a 3 mm diameter pyrolytic graphite edge (PGE) working electrode (Bio-Logic). The electrode surface was activated between measurements by manually polishing its surface for 60 s in a 1.0 μm diamond/water slurry on a diamond polishing pad (Bio-Logic) followed by 60 s in a 0.05 μm alumina/water slurry on a microcloth pad (Bioanalytical systems Inc.). The electrode was rinsed with an excess of methanol followed by milli-Q water directed against the surface of the electrode. Measurements were taken immediately following the polishing procedures. The electrochemical cell was also fitted with a pH electrode (Microelectrodes Inc.) connected to a SevenMulti pH meter (Mettler Toledo). The pH electrode was disconnected from the pH meter during the active measurements to avoid the risk of introducing electric noise. The response and reproducibility of the fully assembled electrochemical cell were checked at the beginning of each experimental day by using standard samples and settings. iR compensation was performed by using the Autolab positive feedback function. Potentials are given versus the normal hydrogen electrode (NHE). All samples were prepared from ultrapure chemicals and the measurements performed under an argon atmosphere. Salt and protein concentration series were obtained by equal-volume titrations. Data processing and analyses were performed using Autolab GPES, KaleidaGraph (Synergy Software), and PeakFit (Systat Software Inc.).

RESULTS

Solution NMR Structure of 2MP-α_3C. A key criterion for the α_3X model system is that the constructed macromolecules are valid biomimics for natural proteins. Heteronuclear multidimensional NMR spectroscopy was employed to confirm that this standard holds for 2MP-α_3C. Sample conditions and experiments used for obtaining resonance assignments and experimental restraints are described in Materials and Methods. The resonance assignments of 2MP-α_3C were essentially complete (99% of backbone atoms and 96% of side chain atoms) and have been deposited at the BMRB (entry 18703). The NOE distance, backbone dihedral angle, and H-bond restraints employed for the structure calculations are summarized in Table 1. CNS was used to calculate trial structures by simulated annealing molecular dynamics.[42] The calculations were based on an average of 14.8 experimental restraints per residue, of which 2.9 represent long-range interhelical distances. The collection of calculated trial structures was evaluated and refined using the CNS accept.inp script to generate the final 32-member ensemble that represents the solution structure of 2MP-α_3C. Figure 2 illustrates 2MP-α_3C as a main chain superposition of the deposited structural ensemble (PDB entry 2LXY) and as a ribbon cartoon displaying the 2-mercaptophenol-C32 (2MP-C32) side chain. The structure is of excellent quality and displays minimal deviations from experimental restraints and idealized covalent geometries, as shown in Table 1. The root-mean-square deviation (rmsd) from the mean coordinates is 0.46 Å for backbone atoms and 0.95 Å when all heavy atoms are included. MOLMOL[43] identified three α-helices, and they are colored

Table 1. Experimental Restraints and Structural Statistics for the Solution NMR 2MP-α_3C Structure

no. of experimental restraints	
NOE, intraresidue	216
NOE, sequential ($\|i - j\| = 1$)	222
NOE, medium-range ($1 < \|i - j\| < 5$)	181
NOE, long-range ($\|i - j\| \geq 5$)	190
NOE restraints, all	809
backbone dihedral angles	107
hydrogen bonds	44
experimental restraints, all	960
restraints per residue	14.8
long-range restraints per residue	2.9
no. of residual restraint violations	
NOE distance of >0.1 Å	0
backbone dihedral angle of >2°	0
no. of structures in ensemble	32
rmsd from experimental restraints	
NOE distance deviation (Å)	0.0061 ± 0.0003
maximal NOE distance deviation (Å)	0.079
backbone angle deviation (deg)	0.221 ± 0.019
maximal backbone angle deviation (deg)	1.2
rmsd from idealized covalent geometry	
bonds (Å)	0.0011 ± 0.0001
angles (deg)	0.331 ± 0.004
impropers (deg)	0.202 ± 0.009
Ramachandra plot statistics (%)	
most favored regions	96.4
additionally allowed regions	3.2
generously allowed regions	0.3
disallowed regions	0
rmsd from average coordinates (Å)	
backbone atoms (residues 1−65)	0.464
all heavy atoms (residues 1−65)	0.949
backbone atoms (residues 2−17, 24−41, 48−64)	0.273
all heavy atoms (residues 2−17, 24−41, 48−64)	0.901

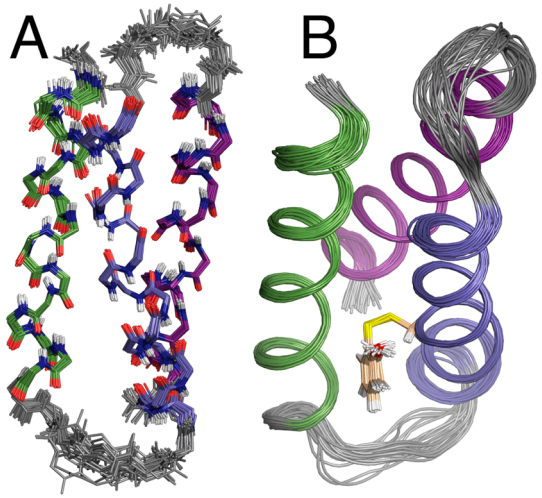

Figure 2. Solution NMR structure of 2MP-α_3C displayed (A) as a backbone (N, H, C, O, and CA) superposition of the final ensemble of 32 simulated annealing structures and (B) as a ribbon cartoon with the side chain of the modified 2-mercaptophenol-C32 (2MP-C32) residue. Helix 1 (residues V2−K17) is colored green, helix 2 (R24−E41) blue, and helix 3 (V48−K64) purple. Nonhelical loop regions are colored gray. See Table 1 for a summary of the NMR experimental restraints and structural statistics.

green (residues V2−K17), blue (R24−E41), and purple (V48−K64) in Figure 2. For the α-helical regions, the rmsd is 0.27 Å for backbone atoms and 0.90 Å for all heavy atoms. The protein is 78% α-helical (51 of 65 residues), which is consistent with earlier CD measurements of 2MP-α_3C (78−81% helical[30]) and the NMR structure of α_3W (51 helical residues of 65 in total[29]). Helices in structured proteins are characterized by a uniformly stable central region flanked by stretches of decreasing stability that give rise to increasing hydrogen exchange rates,[49] more extensive averaging of the three-bond HN−HA J coupling constants dependent upon backbone torsion angles,[50] and an increasing random coil index (RCI[44]). This pattern is clearly observed for the $^3J_{HNHA}$ coupling constants[39] and RCI values[44] obtained for 2MP-α_3C (Table S2 of the Supporting Information).

The formation of an α-helical bundle is largely driven by the hydrophobic residues that are placed in the heptad a and d positions (shown in bold in Scheme 1[28]). These residues are predicted to form stacked three-residue packing layers that together constitute a significant part of the protein hydrophobic core. A solvent accessible surface area (SASA) analysis of the 2MP-α_3C structure is presented in Tables S3 and S4 of the Supporting Information. The heptad a and d residues form a consistent pattern of low SASA values (Table S3 of the Supporting Information). The protein core contains overall six stacked interhelical layers: (V2, L42, V48), (L5, I39, V51), (V9, L35, V55), (L12, 2MP-C32, L58), (V16, L28, I62), and (L19, I25, L65). Figure 3 displays the (V16, L28, I62) and (V9, L35, V55) core layers as an illustration. The average rmsd from the mean coordinates is 0.49 Å for the heavy atoms in these 18 residues. Thus, the hydrophobic core of 2MP-α_3C is highly structured and well-defined.

Architecture of the Phenol Radical Site. The 2MP-C32 side chain is found sandwiched between helices 1 and 2 (Figure 2B). The buried position of the C32 residue (SASA of 0 ± 0%) forces the polar OH group of the attached phenol inside the protein, as designed. The average SASA values for the atoms associated with 2MP-C32 are summarized in Figure 4 and listed in more detail in Table S4 of the Supporting Information. The average SASA values across the structural ensemble are 3.5 ± 0.7% for the whole residue, 2.0 ± 3.1% for the phenol oxygen, and 4.0 ± 5.4% for the phenol hydroxyl proton. The NMR structure also reveals that the phenol is involved in an interhelical hydrogen bond to E13 (Figure 4B). The phenol oxygen−E13 carboxyl oxygen distance is 3.2 ± 0.5 Å across the NMR family of structures. E13 has an average SASA of 12.1 ± 2.6%, which is significantly smaller than those of the other 16 Glu residues in 2MP-α_3C (Table S3 of the Supporting Information). On the atom level, the solvent exposure is located at the carboxyl carbon and oxygen atoms [CD, OE1, and OE2 (Figure 4B and Table S4 of the Supporting Information)]. Interestingly, this suggests a proton-transfer pathway between the buried phenol OH and the bulk solvent via the E13 carboxyl group. The impact of this interaction on the phenol redox chemistry will be the focus of follow-up voltammetry studies. However, a first step is to show that 2MP-α_3C is an electrochemically reversible system. This is demonstrated below.

SWV Analysis of 2MP-α_3C. Square-wave voltammetry (SWV) is a sensitive and diagnostic method for the investigation of various electrochemical processes. Analytical procedures for studying adsorption or diffusion-controlled reversible, quasi-reversible, and irreversible electrode processes

dx.doi.org/10.1021/bi301613p | Biochemistry 2013, 52, 1409−1418

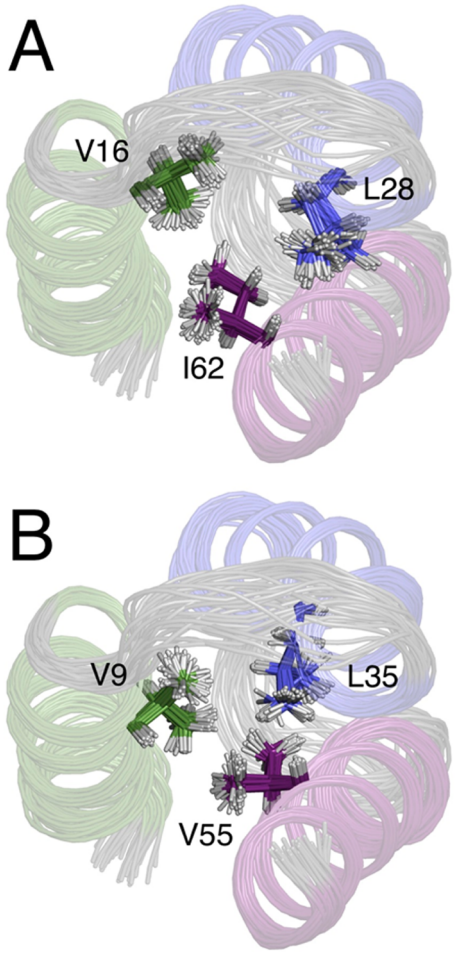

Figure 3. Residues (A) V16, L28, and I62 and (B) V9, L35, and V55 participate in two of the six interhelical packing layers that form a major part of the 2MP-α_3C hydrophobic core.

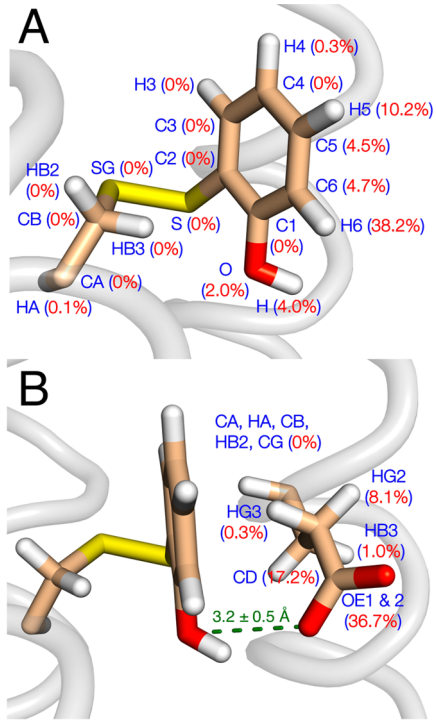

Figure 4. Average solvent accessible surface areas for atoms associated with the hydrogen-bonded 2MP-C32 and E13 pair (see Table S4 of the Supporting Information for additional SASA information). The average O−O distance between the phenol oxygen and the closest E13 carboxyl oxygen is 3.2 ± 0.5 Å. (A) The nomenclature used for 2MP-C32 is based on labeling the modified cysteine/phenol residue as an unnatural tyrosine analogue with backbone atoms derived from C32 and side chain atoms derived from both C32 and the S−S ligated phenol. For the deposited data, convention requires that the covalently attached phenol be labeled as a ligand (name HTS, sequence residue number 101). Table S1 of the Supporting Information provides a guide correlating the residue and atom designations used in the BMRB and PDB with the nomenclature used here and in ref 30. (B) The E13 SASA pattern suggests a proton-transfer pathway between the buried phenol OH via the E13 carboxyl group and the bulk solution.

are well-documented.[46−48] Theoretical methods have been developed to simulate electrode processes that are coupled to preceding or following homogeneous chemical reactions.[51−54] In SWV, the applied potential is stepped progressively in fixed increments (E_{step}), and at each increment, a forward (in this study, oxidative) potential pulse is applied followed by a reverse (reductive) pulse. The current is sampled at the end of each alternating pulse and traced out as a function of E_{step}. This generates a forward (I_{for}), a reverse (I_{rev}), and a net ($I_{net} = I_{for} - I_{rev}$) voltammogram. The SW frequency ($f = {}^1/_2t_p$) determines the length of the applied pulse (t_p). t_p represents the effective time scale of the experiment and can technically be varied between 62.5 ms (8 Hz) and 250 μs (2000 Hz).

2MP-α_3C was expected to follow an EC mechanism in which the observed voltammogram reflects electrode-driven electron transfers, coupled protonic reactions at the phenol oxygen, and possible side reactions by the generated radical. The key purpose here was to identify a frequency range in which the influence on the voltammogram by the putative radical side reactions is small or removed altogether (i.e., where $t_p \ll t_{1/2}$ associated with the radical side reactions). Voltammograms generated under such conditions will be dominated by the thermodynamic and kinetic properties of the electrode process (i.e., phenol PCET) and not by homogeneous side reactions. The SWV analysis involved optimization and characterization of the 2MP-α_3C Faradaic current followed by the collection of SW frequency data series.

2MP-α_3C/PGE Electrode Optimization and Evaluation. The electrochemical analysis of 2MP-α_3C required a pyrolytic graphite "edge" (PGE) working electrode to generate SWV data with good a signal-to-noise (S/N) ratio. A set of experiments was conducted to optimize and characterize the Faradaic response from 2MP-α_3C on a PGE electrode. These studies are described in detail in the Supporting Information and provided the following key results. (i) The mixture of 20 mM APB (acetate, phosphate, borate) buffer, 40−140 mM KCl, and 20−100 μM protein yield voltammograms with optimal S/N ratios at both acidic and alkaline pH (Figure S1 of the Supporting Information). Under these conditions, (ii) E_{peak} is not influenced by the chemical groups present at the electrode surface (Figure S1A,B of the Supporting Information), (iii) diffusion-controlled electrode kinetics is observed (Figure S1C of the Supporting Information), (iv) 2MP-α_3C does not unfold on the electrode surface, and (v) the oxidized protein is not involved in intermolecular radical−radical or radical−substrate reactions (Figure S1B of the Supporting Information). Square-wave voltammograms were collected on 2MP-α_3C, α_3C (i.e., the protein scaffold without the ligated

dx.doi.org/10.1021/bi301613p | *Biochemistry* 2013, 52, 1409−1418

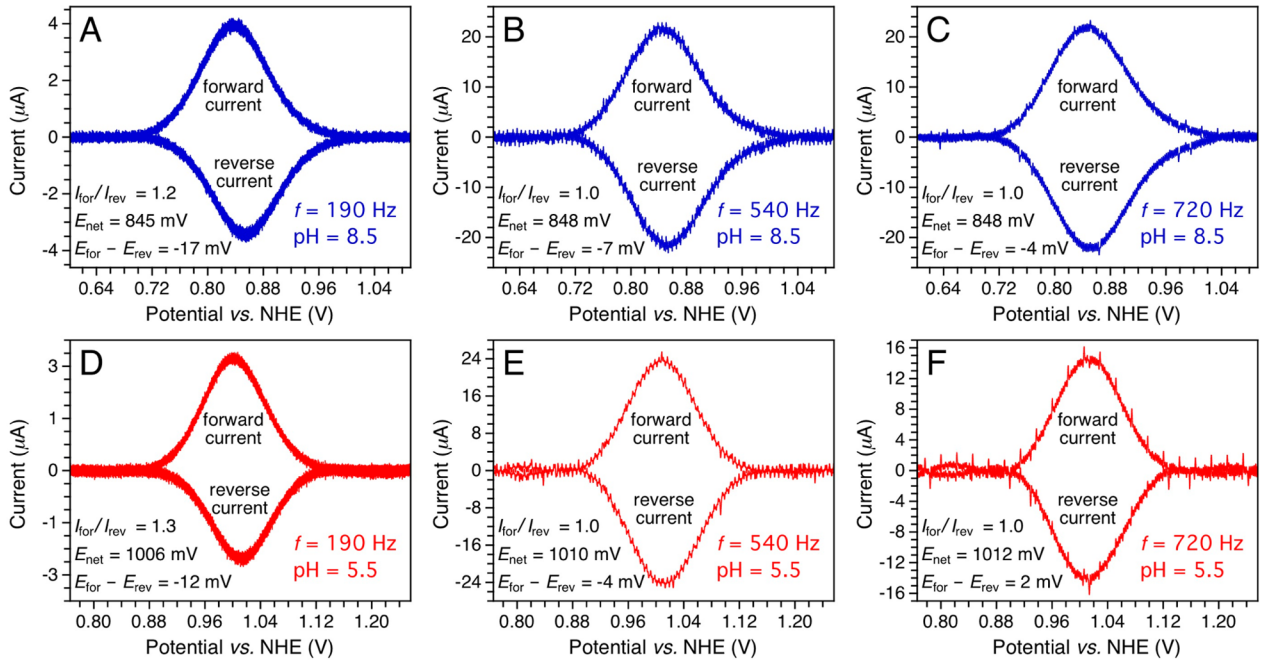

Figure 5. Background-corrected forward and reverse square-wave voltammograms obtained from 2MP-α_3C using a SW frequency of (A and D) 190 Hz (t_p = 2.6 ms), (B and E) 540 Hz (t_p = 926 μs), and (C and E) 720 Hz (t_p = 694 μs). The voltammograms displayed in panels A–C were obtained at pH 8.51 ± 0.02 and those displayed in panels D–F at pH 5.52 ± 0.01. SWV settings: 75 μM 2MP-α_3C in 20 mM APB, 80 mM KCl; PGE working electrode; temperature, 25 °C; step potential, 0.15 mV; SW pulse amplitude, 25 mV.

phenol), and plain buffer under the conditions optimized for the PGE electrode (Figure S2 of the Supporting Information). Consistent with the assignment of the voltammogram to the protein-bound phenol,[30] a Faradaic current is uniquely observed for 2MP-α_3C while the α_3C voltammograms closely resemble the baseline buffer traces. A high level of reproducibility was observed for data replicates and independently obtained 2MP-α_3C voltammograms (Figure S4 of the Supporting Information). The average errors in E_{peak} (≤±5 mV) and half-height peak widths (≤±5 mV) were small. The peak amplitude and the S/N ratio are both sensitive to the SW frequency with a small Faradaic current at low frequencies (≤60 Hz) and an increase in noise at high frequencies (≥540 Hz). The average error in I_{net} was approximately ±10%.

2MP-α_3C Gives Rise to Reversible Phenol Voltammograms. Figure 5 shows background-corrected forward and reverse SW voltammograms collected at 190, 540, and 720 Hz at pH 8.51 (top row) and pH 5.52 (bottom row). The forward and reverse voltammograms represent the oxidative and reductive currents, respectively. The two pH data sets display the same trend of changing from quasi-reversible to reversible as the frequency increases. E_{net} is highly insensitive to the frequency and increases by only 3 ± 2 mV (pH 8.51) and 6 ± 2 mV (pH 5.52) as the frequency is changed from 190 to 720 Hz. The I_{for}/I_{rev} ratio decreases from 1.2 (pH 8.51) and 1.3 (pH 5.52) to a limiting value of 1.0 at ≥540 Hz. ΔE ($=E_{for} - E_{rev}$) decreases from −17 ± 2 to −4 ± 2 mV (pH 8.51) and from −12 ± 2 to 2 ± 2 mV (pH 5.52). Figure 6 illustrates the changes in the properties of the high-pH 2MP-α_3C voltammogram in more detail and over a broader frequency range (30–720 Hz). Figure 6A shows that E_{net} is 847 ± 2 mV (over a 120–720 Hz range), E_{for} is 844 ± 2 mV (440–720 Hz), and E_{rev} is 851 ± 2 mV (440–720 Hz) at pH 8.51 ± 0.01. This is consistent with a fully reversible diffusion-controlled electrode process, which is characterized by peak potentials that are independent of the SW frequency and separated by only a few millivolts.[47,48] Figure 6B shows that I_{net} increases as a function of the frequency and reaches a maximum in the 440–720 Hz range. This observation is consistent with SWV simulations of EC systems in which the coupled chemical reactions are so slow relative to the time scale of the experiment that they have no impact on the voltammogram.[51−54] We also observe that the I_{for}/I_{rev} ratio declines as the frequency increases and reaches a limiting value of 1.0 at ≥440 Hz (Figure 6C). We conclude that the 2MP-α_3C electrode process is reversible at SW frequencies above ∼500 Hz at both pH 8.5 and 5.5.

DISCUSSION

Tyrosine oxidation and reduction occurs as a PCET process in which the loss or gain of e^- or H^+ may take place as a single event [concerted electron proton transfer (CEPT)] or follow a stepwise pathway (electron proton transfer or proton electron transfer). CEPT avoids high-energy intermediates but requires a spatially well-organized site. The larger mass of the proton relative to the electron makes the proton-tunneling component of the CEPT process highly dependent on structural details. The electron and proton acceptor and donor can be separate molecules or a single molecular center. Examples of the former situation include oxidation of Y_Z and Y_D in photosystem II (the photo-oxidized chlorophyll complex $P680^+$ serves as the oxidant; a H-bonded His serves as the primary proton acceptor[1,55−57]) and oxidation and reduction of Y356-β in *E. coli* ribonucleotide reductase (multistep ET via Y356-β; proton acceptor and donor possibly E350-β[58,59]). An example of the latter situation includes, e.g., reduction of the catalytically active Y385 radical in prostaglandin H synthase (net transfer of e^- or H^+ from the fatty acid substrate to Y385-$O^{\bullet}$[60]). The general consensus emerging from studies on enzymes and model systems is that tyrosine oxidation, and most likely also the reduction, occurs as a CEPT process in the majority of

dx.doi.org/10.1021/bi301613p | *Biochemistry* 2013, 52, 1409−1418

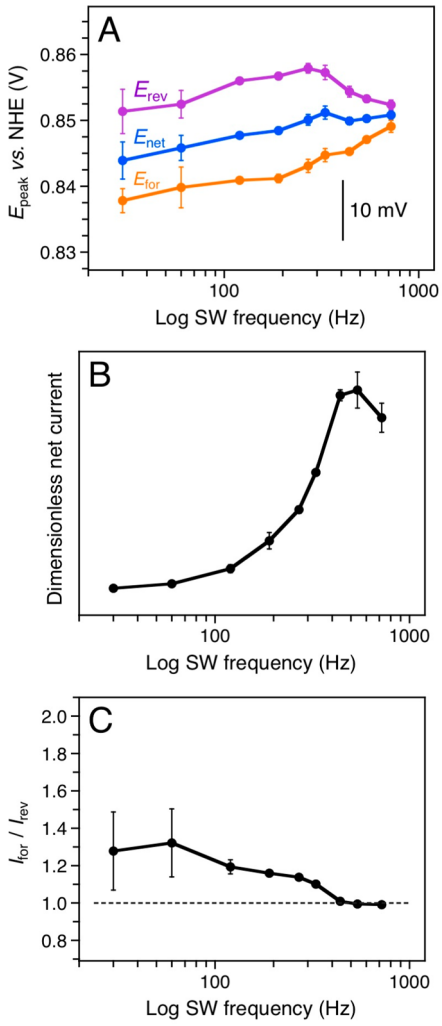

Figure 6. Changes in the (A) peak potential of the net (E_{net}), forward (E_{for}), and reverse (E_{rev}) 2MP-α_3C voltammogram as a function the SW frequency. (B) Dimensionless I_{net} and (C) I_{for}/I_{rev} ratio as a function of the SW frequency. The dimensionless net current was calculated as described in ref 46 and using a diffusion coefficient of $(1.4 \pm 0.2) \times 10^{-6}$ cm^2 s^{-1} (Figure S5 of the Supporting Information). SWV settings: 75 μM 2MP-α_3C in 20 mM APB, 80 mM KCl, pH 8.51 ± 0.02; PGE working electrode; temperature, 25 °C; step potential, 0.15 mV; SW pulse amplitude, 25 mV.

systems.[18] The MP-α_3C proteins were constructed to electrochemically characterize phenol oxidation and reduction in a structured protein environment with specific emphasis on the protonic reactions occurring at the phenol oxygen.[30] This study describes several significant steps toward this goal, as discussed below.

2MP-α_3C Displays Key Biomimetic Properties. 2MP-α_3C is a stable, uniquely structured three-helix bundle with a well-defined hydrophobic core. The model protein displays structural characteristics that are fully consistent with properties observed for native proteins. We note that the structural ensemble of an aqueous "peptide" would typically reflect a population distributed across a more shallow energy landscape relative to the energy landscape of a uniquely structured protein. Consequently, a radical generated in a peptide scaffold resides in an environment in which structural interactions and solvent exposure are less well-defined and less well-controlled. The classic "protein" properties observed for 2MP-α_3C are likely to play a significant role in the stabilization of the radical state (vide infra).

2MP-α_3C was designed to specifically shield the phenol OH group from the bulk solvent (Figure 1A).[30] The solution NMR structure of 2MP-α_3C verifies the design of the radical site (Figure 4A). Only 3.5 ± 0.7% of 2MP-C32 is solvent-exposed, and the phenol OH group has an average SASA of 3.0 ± 4.5% (Table S4 of the Supporting Information). The NMR structure also reveals that the phenol forms an interhelical hydrogen bond to E13 (Figure 4B). It is likely that E13 is involved in rapid de- and/or reprotonation reactions associated with the electrode-driven oxidation and reduction of 2MP-C32. As discussed below, the pH dependence of the 2MP-C32 potential is consistent with an overall charge neutral system; i.e., the phenol site is in equilibrium with the bulk phase on the time scale of the experiment. The SASA analysis shows that the levels of solvent exposure of the phenol OH and the carboxyl oxygens of E13 (37 ± 18%) differ by 1 order of magnitude. This suggests a redox-driven proton-transfer pathway between the phenol and the bulk solvent. These structural features are most likely tightly connected to the electrochemical reversibility of the phenol oxidation−reduction process. Investigation of these issues is in progress.

Reversible Phenol Voltammograms Provide Formal Reduction Potentials. For a reversible and diffusion-controlled redox system, the peak potential of the SWV net current (E_{net}) equals the formal reduction potential ($E^{\circ\prime}$) when the reduced and oxidized species diffuse at equal rates.[46] The diffusion coefficient of reduced 2MP-α_3C was determined to $(1.4 \pm 0.2) \times 10^{-6}$ cm^2 s^{-1} by pulsed field gradient NMR (Figure S5 of the Supporting Information).[35] α_3Y exhibits the same rate of diffusion,[31] which is typical of a small globular protein. The diffusion coefficient of 2MP-α_3C is not expected to change significantly as a function of redox state (loss or gain of one e$^-$ and H$^+$). We conclude that E_{net} (≥500 Hz) represents the formal reduction potential of the protein-bound phenol.

The initial characterization of 2MP-α_3C included a differential pulse voltammetry (DPV) study using a glassy carbon (GC) working electrode.[30] The DPV/GC study provided three key results. The α_3C scaffold is redox inert (no Faradaic current observed); the protein-bound phenol is redox-active (Faradaic current observed upon phenol ligation), and the 2MP-α_3C voltammogram represents the neutral phenol-O$^\bullet$/phenol-OH redox pair (ΔE_{peak} = 55 ± 5 mV/pH unit). DPV and SWV are both sensitive methods (minimization of capacitative background currents, peak-shaped response), but only the latter provides a diagnostic tool similar to that of cyclic voltammetry.[46] Thus, the preliminary DPV/GC study of 2MP-α_3C[30] did not delineate the electrode process or exclude the possibility of distorting protein−electrode interactions. Here a pyrolytic graphite edge (PGE) working electrode system was optimized for 2MP-α_3C, which allowed a SWV analysis to be performed. The SWV study reproduced the three DPV results listed above (Figure S2 of the Supporting Information and Figure 5; ΔE_{net} = 54 ± 5 mV/pH unit). In addition, we could show that (i) E_{net} is not influenced by chemical groups on the working electrode surface, (ii) the protein does not unfold on the electrode surface, (iii) the electrode process is reversible and (iv) diffusion-controlled, and (v) E_{net} (≥500 Hz) = $E^{\circ\prime}$. Comparing the 2MP-α_3C $E_{1/2}$ potential measured with DPV, using either a GC[30] or a PGE (Figure S1A of the Supporting Information) electrode, with $E^{\circ\prime}$ as determined by SWV reveals

dx.doi.org/10.1021/bi301613p | Biochemistry 2013, 52, 1409−1418

that there is no significant difference (9 ± 12 mV). The potential is not influenced by the electrode surface, and both DPV and SWV provide the thermodynamically corrected formal potential of the 2MP-α_3C redox system.

2MP-α_3C was made as an analogue for tyrosine radical proteins, and $E^{\circ\prime}$ values observed for this system are close to those observed for α_3Y.[31] $E^{\circ\prime}$(pH 8.51 ± 0.02) is 847 ± 2 mV versus NHE for the phenol-O$^\bullet$/phenol-OH redox couple. This value is ~60 mV lower than the $E^{\circ\prime}$ of 909 ± 3 mV for the Y32-O$^\bullet$/Y32-OH redox pair at the same pH. Thus, both the structural and redox properties of 2MP-α_3C make this protein highly suitable as a biomimetic system for natural tyrosine redox cofactors.

2MP-α_3C Contains a Long-Lived Phenol Radical. The redox reversibility observed for 2MP-α_3C is rare for a phenol-based system. Solvated tyrosine or phenol gives rise to irreversible voltammograms dominated by rapid intermolecular radical−radical and radical−substrate reactions.[61−63] Some sterically protected and H-bonded phenols dissolved in organic solvents give rise to voltammograms that are quasi-reversible to various degrees (e.g., refs 19−25). Such voltammograms reflect electrode-driven oxidation and reduction, coupled protonic reactions at the phenol oxygen, and/or radical side reactions. The 2MP-α_3C voltammogram becomes fully reversible at ~500 Hz, and under these conditions, neither protonic reactions nor radical side reactions influence the observed voltammogram. Voltammograms collected at <500 Hz are quasi-reversible, and this fact may arise from the coupled protonic reactions and/or radical side reactions. These observations are consistent with a very long-lived radical state, even if the quasi-reversibility arises mainly from radical side reactions. SWV simulations predict that the influence of coupled chemical reactions on E_{net} approaches zero when $\log(2t_p k_{EC}) \leq -1.5$.[47,51,52] There is no significant change in the E_{net} of >120 Hz at high pH. This predicts that the rate constant (k_{EC}) associated with side reaction(s) is $\leq 4\ s^{-1}$, which translates into a radical $t_{1/2}$ of ≥180 ms. This is a remarkably long lifetime for an oxidized phenol and still represents only a lower-limit estimate. A similar observation was made for Y32-O$^\bullet$, which has a $t_{1/2}$ of ≥30 ms.[31] To provide a comparison, aqueous tyrosine has a radical $t_{1/2}$ of ~10−20 μs under the conditions used here.[62] These results highlight the difference between solution redox chemistry and protein redox chemistry.

Concluding Remarks. 2MP-α_3C was created to gain insights into tyrosine radical cofactors. 2MP-α_3C mimics the biochemical systems in several important ways. It displays structural properties associated with natural proteins. The radical site is shielded and the phenol H-bonded to a Glu. It is generally accepted that the properties of tyrosine redox cofactors critically depend on interactions with a H-bonded proton acceptor or donor. The phenol oxidation−reduction cycle is reversible and occurs in a well-structured environment. The protein matrix stabilizes the radical into the high-millisecond time scale or longer. Most, if not all, PCET-oriented mechanistic studies of tyrosine/phenol model systems have focused on the oxidation side of the redox cycle.[18] Loss of the radical state in various side reactions naturally makes it more difficult to investigate the reduction process. 2MP-α_3C provides the unique opportunity to study the electron and proton transfers associated with the reduction process.

■ ASSOCIATED CONTENT

Ⓢ Supporting Information

2MP-α_3C/PGE working electrode optimization and control experiments (Figures S1−S4), diffusion attenuation plot (Figure S5), designations used for the unnatural 2MP-C32 residue (Table S1), $^3J_{HNHA}$ coupling constants and Random Coil Index values obtained for 2MP-α_3C (Table S2), SASA values for all 2MP-α_3C residues (Table S3), and atom-level SASA values for 2MP-C32 and E13 (Table S4). This material is available free of charge via the Internet at http://pubs.acs.org.

Accession Codes

PDB entry 2LXY and BMRB entry 18703.

■ AUTHOR INFORMATION

Corresponding Author

*Address: 905 Stellar-Chance Laboratories, Department of Biochemistry and Biophysics, University of Pennsylvania, 422 Curie Blvd., Philadelphia, PA 19104-6059. Telephone: (215) 746-2444. Fax: (215) 573-7290. E-mail: tommos@mail.med.upenn.edu.

Funding

Funding was provided by National Institutes of Health (NIH) Grant GM079190 and by NIH Predoctoral Fellowship GM096756 to M.C.M.-R.

Notes

The authors declare no competing financial interest.

■ ABBREVIATIONS

α_3Y, α_3W, and α_3C, de novo protein containing a single buried tyrosine, tryptophan, and cysteine, respectively; APB buffer, sodium acetate, potassium phosphate, sodium borate buffer; DPV, differential pulse voltammetry; DSS, 4,4-dimethyl-4-silapentane-1-sulfonic acid; $E^{\circ\prime}$, formal potential; $E_{1/2}$, voltammetry half-wave potential; EC, electrode process coupled to homogeneous chemical reaction; E_{peak}, peak potential; E_{for}, E_{rev}, and E_{net}, peak potential of the forward, reverse, and net currents, respectively, in SWV; f, square-wave frequency; GC, glassy carbon; pK_{app}, apparent pK_a value; I_{for}, I_{rev}, and I_{net}, forward, reverse, and net currents, respectively, in SWV; MP, mercaptophenol; PSII, photosystem II; PCET, proton-coupled electron transfer; PGE, pyrolytic graphite edge; SWV, square-wave voltammetry; t_p, pulse width; Y32, redox-active tyrosine in α_3Y; Y_Z and Y_D, redox-active tyrosines in photosystem II.

■ REFERENCES

(1) Tommos, C., and Babcock, G. T. (2000) Proton and hydrogen currents in photosynthetic water oxidation. *Biochim. Biophys. Acta 1458*, 199−219.

(2) Pesavento, R. P., and van der Donk, W. A. (2001) Tyrosyl radical cofactors. *Adv. Protein Chem. 58*, 317−385.

(3) Hoganson, C. W., and Tommos, C. (2004) The function and characteristics of tyrosyl radical cofactors. *Biochim. Biophys. Acta 1655*, 116−122.

(4) Reece, S. Y., and Nocera, D. G. (2009) Proton-coupled electron transfer in biology: Results from synergistic studies in natural and model systems. *Annu. Rev. Biochem. 78*, 673−699.

(5) Dempsey, J. L., Winkler, J. R., and Gray, H. B. (2010) Proton-coupled electron flow in protein redox machines. *Chem. Rev. 110*, 7024−7039.

(6) Cukier, R. I., and Nocera, D. G. (1998) Proton-coupled electron transfer. *Annu. Rev. Phys. Chem. 49*, 337−369.

(7) Mayer, J. M. (2004) Proton-coupled electron transfer: A reaction chemist's view. *Annu. Rev. Phys. Chem. 55*, 363−390.

(8) Huynh, M. H. V., and Meyer, T. J. (2007) Proton-Coupled Electron Transfer. *Chem. Rev. 107*, 5004−5064.
(9) Hammes-Schiffer, S., and Stuchebrukhov, A. A. (2010) Theory of coupled electron and proton transfer reactions. *Chem. Rev. 110*, 6939−6960.
(10) Savéant, J.-M. (2012) Electrochemical approach to proton-coupled electron transfers: Recent advances. *Energy Environ. Sci. 5*, 7718−7731.
(11) Sjödin, M., Styring, S., Åkemark, B., Sun, L., and Hammarström, L. (2000) Proton-coupled electron transfer from tyrosine in a tyrosine-ruthenium-tris-bipyridine complex: Comparison with tyrosine$_Z$ oxidation in photosystem II. *J. Am. Chem. Soc. 122*, 3932−3936.
(12) Stubbe, J., Nocera, D. G., Yee, C. S., and Chang, M. C. Y. (2003) Radical initiation in the class I ribonucleotide reductase: Long-range proton-coupled electron transfer? *Chem. Rev. 103*, 2167−2202.
(13) Reece, S. Y., and Nocera, D. G. (2005) Direct tyrosine oxidation using the MLCT excited states of rhenium polypyridyl complexes. *J. Am. Chem. Soc. 127*, 9448−9458.
(14) Fecenko, C. J., Meyer, T. J., and Thorp, H. H. (2006) Electrocatalytic oxidation of tyrosine by parallel rate limiting proton transfer and multisite electron-proton transfer. *J. Am. Chem. Soc. 128*, 11020−11021.
(15) Sibert, R., Josowicz, M., Porcelli, F., Veglia, G., Range, K., and Barry, B. A. (2007) Proton-coupled electron transfer in a biomimetic peptide as a model of enzyme regulatory mechanisms. *J. Am. Chem. Soc. 129*, 4393−4400.
(16) Costentin, C., Louault, C., Robert, M., and Savéant, J.-M. (2009) The electrochemical approach to concerted proton-electron transfers in the oxidation of phenols in water. *Proc. Natl. Acad. Sci. U.S.A. 106*, 18143−18148.
(17) Pizano, A. A., Lutterman, D. A., Holder, P. G., Teets, T. S., Stubbe, J., and Nocera, D. G. (2012) Photo-ribonucleotide reductase β2 by selective cysteine labeling with a radical phototrigger. *Proc. Natl. Acad. Sci. U.S.A. 109*, 39−43.
(18) Warren, J. J., Winkler, J. R., and Gray, H. B. (2012) Redox properties of tyrosine and related molecules. *FEBS Lett. 586*, 596−602.
(19) Maki, T., Araki, Y., Ishida, Y., Onomura, O., and Matsumura, Y. (2001) Construction of persistent phenoxyl radical with intramolecular hydrogen bonding. *J. Am. Chem. Soc. 123*, 3371−3372.
(20) Benisvy, L., Blake, A. J., Collison, D., Davies, E. S., Garner, C. D., McInnes, E. J. L., McMaster, J., Whittaker, G., and Wilson, C. (2003) A phenol−imidazole pro-ligand that can exist as a phenoxyl radical, alone and when complexed to copper(II) and zinc(II). *Dalton Trans. 10*, 1975−1985.
(21) Rhile, I. J., and Mayer, J. M. (2004) One-electron oxidation of a hydrogen-bonded phenol occurs by concerted proton-coupled electron transfer. *J. Am. Chem. Soc. 126*, 12718−12719.
(22) Costentin, C., Robert, M., and Savéant, J.-M. (2006) Electrochemical and homogeneous proton-coupled electron transfers: Concerted pathways in the one-electron oxidation of a phenol coupled with an intramolecular amine-driven proton transfer. *J. Am. Chem. Soc. 128*, 4552−4553.
(23) Rhile, I. J., Markle, T. F., Nagao, H., DiPasquale, A. G., Lam, O. P., Lockwood, M. A., Rotter, K., and Mayer, J. M. (2006) Concerted proton-electron transfer in the oxidation of hydrogen-bonded phenols. *J. Am. Chem. Soc. 128*, 6075−6088.
(24) Moore, G. F., Hambourger, H., Gervaldo, M., Poluektov, O. G., Rajh, T., Gust, D., Moore, T. A., and Moore, A. L. (2008) A Bioinspired Construct That Mimics the Proton Coupled Electron Transfer between P680$^{\bullet+}$ and the Tyr$_Z$-His190 Pair of Photosystem II. *J. Am. Chem. Soc. 130*, 10466−10467.
(25) Zhang, M.-T., Irebo, T., Johansson, O., and Hammarström, L. (2011) Proton-coupled electron transfer from tyrosine: A strong rate dependence on intermolecular proton transfer distance. *J. Am. Chem. Soc. 133*, 13224−13227.
(26) Tommos, C., Skalicky, J. J., Pilloud, D. L., Wand, A. J., and Dutton, P. L. (1999) De novo proteins as models of radical enzymes. *Biochemistry 38*, 9495−9507.
(27) Westerlund, K., Berry, B. W., Privett, H. K., and Tommos, C. (2005) Exploring amino-acid radical chemistry: Protein engineering and de novo design. *Biochim. Biophys. Acta 1707*, 103−116.
(28) DeGrado, W. F., Summa, C. M., Pavone, V., Nastri, F., and Lombardi, A. (1999) De novo design and structural characterization of proteins and metalloproteins. *Annu. Rev. Biochem. 68*, 779−819.
(29) Dai, Q.-H., Tommos, C., Fuentes, E. J., Blomberg, M. R. A., Dutton, P. L., and Wand, A. J. (2002) Structure of a de novo designed model protein of radical enzymes. *J. Am. Chem. Soc. 124*, 10952−10953.
(30) Hay, S., Westerlund, K., and Tommos, C. (2005) Moving a phenol hydroxyl group from the surface to the interior of a protein: Effects on the phenol potential and pK_A. *Biochemistry 44*, 11891−11902.
(31) Berry, B. W., Martínez-Rivera, M. C., and Tommos, C. (2012) Reversible voltammograms and a Pourbaix diagram for a protein tyrosine radical. *Proc. Natl. Acad. Sci. U.S.A. 109*, 9739−9743.
(32) Martínez-Rivera, M. C., Berry, B. W., Valentine, K. G., Westerlund, K., Hay, S., and Tommos, C. (2011) Electrochemical and structural properties of a protein system designed to generate tyrosine Pourbaix diagrams. *J. Am. Chem. Soc. 133*, 17786−17795.
(33) Neri, D., Szyperski, T., Otting, G., Senn, H., and Wüthrich, K. (1989) Stereospecific nuclear magnetic resonance assignments of the methyl groups of valine and leucine in the DNA-binding domain of the 434 repressor by biosynthetically directed fractional ^{13}C labeling. *Biochemistry 28*, 7510−7516.
(34) Ellman, G. L. (1959) Tissue sulfhydryl groups. *Arch. Biochem. Biophys. 82*, 70−77.
(35) Zheng, G., and Price, W. S. (2009) Simultaneous convection compensation and solvent suppression in biomolecular NMR diffusion experiments. *J. Biomol. NMR 45*, 295−299.
(36) Sattler, M., Schleucher, J., and Griesinger, C. (1999) Heteronuclear multidimensional NMR experiments for the structure determination of proteins in solution employing pulsed field gradients. *Prog. Nucl. Magn. Reson. Spectrosc. 34*, 93−158.
(37) Moseley, H. N. B., Sahota, G., and Montelione, G. T. (2004) Assignment validation software suite for the evaluation and presentation of protein resonance assignment data. *J. Biomol. NMR 28*, 341−355.
(38) Cornilescu, G., Delaglio, F., and Bax, A. (1999) Protein backbone angle restraints from searching a database for chemical shift and sequence homology. *J. Biomol. NMR 13*, 289−302.
(39) Vuister, G. W., and Bax, A. (1993) Quantitative *J* correlation: A new approach for measuring homonuclear three-bond J(H^{N}H$^\alpha$) coupling constants in ^{15}N-enriched proteins. *J. Am. Chem. Soc. 115*, 7772−7777.
(40) Clore, G. M., Kay, L. E., Bax, A., and Gronenborn, A. M. (1991) Four-dimensional ^{13}C/^{13}C-edited Nuclear Overhauser Enhancement Spectroscopy of a Protein in Solution: Application of Interleukin 1β. *Biochemistry 30*, 12−18.
(41) Goddard, T. D., and Kneller, D. G. (2008) *SPARKY 3*, University of California, San Francisco.
(42) Brunger, A. T., Adams, P. D., Clore, G. M., DeLano, W. L., Gros, P., Grosse-Kunstleve, R. W., Jiang, J. S., Kuszewski, J., Nilges, M., Pannu, N. S., Read, R. J., Rice, L. M., Simonson, T., and Warren, G. L. (1998) Crystallography & NMR system: A new software suite for macromolecular structure determination. *Acta Crystallogr. D54*, 905−921.
(43) Koradi, R., Billeter, M., and Wüthrich, K. (1996) MOLMOL: A program for display and analysis of macromolecular structures. *J. Mol. Graphics 14*, 51−52.
(44) Berjanskii, M. V., and Wishart, D. S. (2005) A simple method to predict protein flexibility using secondary chemical shifts. *J. Am. Chem. Soc. 127*, 14970−14971.
(45) Parry, E. P., and Osteryoung, R. A. (1965) Evaluation of analytical pulse polarography. *Anal. Chem. 37*, 1634−1637.
(46) Bard, A. J., and Faulkner, L. R. (2001) *Electrochemical methods: Fundamentals and applications*, 2nd ed., John Wiley & Sons, Inc., New York.

(47) Osteryoung, J., and O'Dea, J. J. (1986) Square-wave voltammetry. In *Electroanalytical chemistry* (Bard, A. J., Ed.) Vol. 5, pp 209−308, Marcel Dekker, New York.
(48) Mirčeski, V., Komorsky-Lovrić, Š., and Lovrić, M. (2007) Square-wave voltammetry: Theory and applications. In *Monographs in Electrochemistry* (Scholz, F., Ed.) Springer-Verlag, Berlin.
(49) Wand, A. J., Roder, H., and Englander, S. W. (1986) Two-dimensional ^{1}H-NMR studies of cytochrome-c: Hydrogen-exchange in the N-terminal helix. *Biochemistry 25*, 1107−1114.
(50) Pardi, A., Billeter, M., and Wüthrich, K. (1984) Calibration of the angular dependence of the amide proton-C^{a} proton coupling constants, $^{3}J_{HN\alpha}$, in a globular protein. *J. Mol. Biol. 180*, 741−751.
(51) O'Dea, J. J., Osteryoung, J., and Osteryoung, R. A. (1981) Theory of square wave voltammetry for kinetic systems. *Anal. Chem. 53*, 695−701.
(52) Miles, A. B., and Compton, R. G. (2000) Simulation of square-wave voltammetry: EC and ECE electrode processes. *J. Phys. Chem. B 104*, 5331−5342.
(53) Garay, F., and Milivoj Lovrić, M. (2002) Square-wave voltammetry of quasi-reversible electrode processes with coupled homogeneous chemical reactions. *J. Electroanal. Chem. 518*, 91−102.
(54) Rudolph, M. (2001) Digital simulation with the fast implicit finite difference (FIFD) algorithm. Part 5: Digital simulations of square wave voltammetry for any user defined electrochemical mechanism comprising first- and second-order chemical reactions. *J. Electroanal. Chem. 503*, 15−27.
(55) Hays, A.-M. A., Vassiliev, I. R., Golbeck, J. H., and Debus, R. J. (1999) Role of D1-His190 in the proton-coupled oxidation of tyrosine Y_Z in manganese-depleted photosystem II. *Biochemistry 38*, 11851−11865.
(56) Umena, Y., Kawakami, K., Shen, J.-R., and Kamiya, N. (2011) Crystal structure of oxygen-evolving photosystem II at a resolution of 1.9 Å. *Nature 473*, 55−60.
(57) Keough, J. M., Jenson, D. L., Zuniga, A. N., and Bary, B. A. (2011) Proton coupled electron transfer and redox-active tyrosine Z in the photosynthetic oxygen-evolving complex. *J. Am. Chem. Soc. 133*, 11084−11087.
(58) Reece, S. Y., Hodgkiss, J. M., Stubbe, J., and Nocera, D. G. (2006) Proton-coupled electron transfer: The mechanistic underpinning for radical transport and catalysis in biology. *Philos. Trans. R. Soc. B 1472*, 1351−1364.
(59) Yokoyama, K., Smith, A. A., Corzilius, B., Griffin, R. G., and Stubbe, J. (2011) Equilibration of tyrosyl radicals ($Y_{356}^{\bullet}$, $Y_{731}^{\bullet}$, $Y_{730}^{\bullet}$) in the radical propagation pathway of the *Escherichia coil* class Ia ribonucleotide reductase. *J. Am. Chem. Soc. 133*, 18420−18432.
(60) Tsai, A.-L., and Kulmacz, R. J. (2010) Prostaglandin H synthase: Resolved and unresolved mechanistic issues. *Arch. Biochem. Biophys. 493*, 103−124.
(61) Mahoney, L. R., and DaRooge, M. A. (1975) Kinetic behavior and thermochemical properties of phenoxy radical. *J. Am. Chem. Soc. 97*, 4722−4731.
(62) Hunter, E. P. L., Desrosiers, M. F., and Simic, M. G. (1998) The effect of oxygen, antioxidants, and superoxide radical on tyrosine phenoxyl radical dimerization. *Free Radical Biol. Med. 6*, 581−585.
(63) Ye, M., and Schuler, R. H. (1989) Second-order combination reactions of phenoxyl radicals. *J. Phys. Chem. 93*, 1898−1902.